Broadband Spectral Modeling of the Galactic Globular Cluster Terzan 5

H. Ndiyavala[1,2], C. Venter[1], T. J. Johnson[3], A. K. Harding[4] et al. for the *Fermi* LAT Collaboration

[1] University of Namibia, Khomasdal Campus, Private Bag 13301, Windhoek, Namibia
[2] Centre for Space Research, North-West University, Potchefstroom Campus, Private Bag X6001, Potchefstroom, 2520, South Africa
[3] College of Science, George Mason University, Fairfax, VA 22030, resident at Naval Research Laboratory, Washington, DC 20375, USA
[4] Astrophysics Science Division, NASA Goddard Space Flight Center, Greenbelt, MD 20771, USA

Email: 26403366@nwu.ac.za

ABSTRACT

Terzan 5 is the only Galactic globular cluster plausibly detected at very high energies (VHEs; E > 100 GeV) by the High Energy Stereoscopic System (H.E.S.S.) and has an unexpected, asymmetric morphology offset from the cluster center. We present new continuum radio data from Effelsberg Radio Telescope and the *Fermi* Large Area Telescope on this source. Our fit to the broadband spectral energy distribution assumes that emission originates from a population of embedded millisecond pulsars and their leptonic winds. Our model invokes unpulsed synchrotron and inverse Compton components to model radio and TeV data, cumulative pulsed curvature radiation to fit the *Fermi* data, and cumulative synchrotron emission by electron-positron pairs within the pulsar magnetospheres to explain the hard *Chandra* X-ray spectrum. While our model provides reasonable spectral fits, more and higher-quality spectral and spatial data will help discriminate between competing proposed scenarios for the broadband emission, such as a hadronic (short gamma-ray burst remnant) or white-dwarf origin thereof.

1. INTRODUCTION

Discovered in the 1960s, the Galactic globular cluster (GC) Terzan 5 is a fascinating, nearby object lying at a distance $d = 5.9 \pm 0.5$ kpc (Valenti et al. 2007) and having a particularly high central stellar density as well as high metallicity. It also has the highest stellar interaction rate of all Galactic GCs (Verbunt & Hut 1987), which is probably linked to the large number of X-ray binaries found in this system. Terzan 5 hosts the largest number of millisecond pulsars (37 MSPs) of all Galactic GCs (Cadelano et al. 2018). It is the only GC plausibly detected at VHEs (Anderhub et al. 2009; Aharonian et al. 2009; McCutcheon et al. 2009; Abramowski et al. 2011, 2013) and exhibits an unexpectedly asymmetric morphology which is offset from the cluster center. Terzan 5 has also been detected in radio, X-ray, and GeV γ-ray bands, and therefore given the richness of the existing data set on Terzan 5, as well as the variety of models that exist to explain GC emission, we use this system as a case study to probe the origin of multi-wavelength emission from GCs. Improved models will aid selection of promising GCs for future observations by the Cherenkov Telescope Array (CTA), which may see tens of GCs in the next decade (Ndiyavala 2018). We therefore aimed to gather more data on Terzan 5 and model the updated SED in a leptonic scenario.

2. MULTI-WAVELENGTH DATA AND SPECTRAL UPPER LIMITS

2.1. Previous Radio Observations

Terzan 5 was detected in the NRAO VLA Sky Survey (NVSS) at 21 cm as a single source with a flux of 5 mJy (Condon et al. 1998). Clapson et al. (2011) analysed archival 11 cm and 21 cm Effelsberg data and detected several radio structures in the direction of Terzan 5. However, given the uncertainty in flux, no spectral index could be inferred. Clapson et al. (2011) speculated that one structure in particular (labeled as "Region 11"), extending from the GC center to the north-west (roughly perpendicular to the Galactic Plane), could be the result of synchrotron radiation (SR) by electrons escaping from the large population of MSPs in this GC.
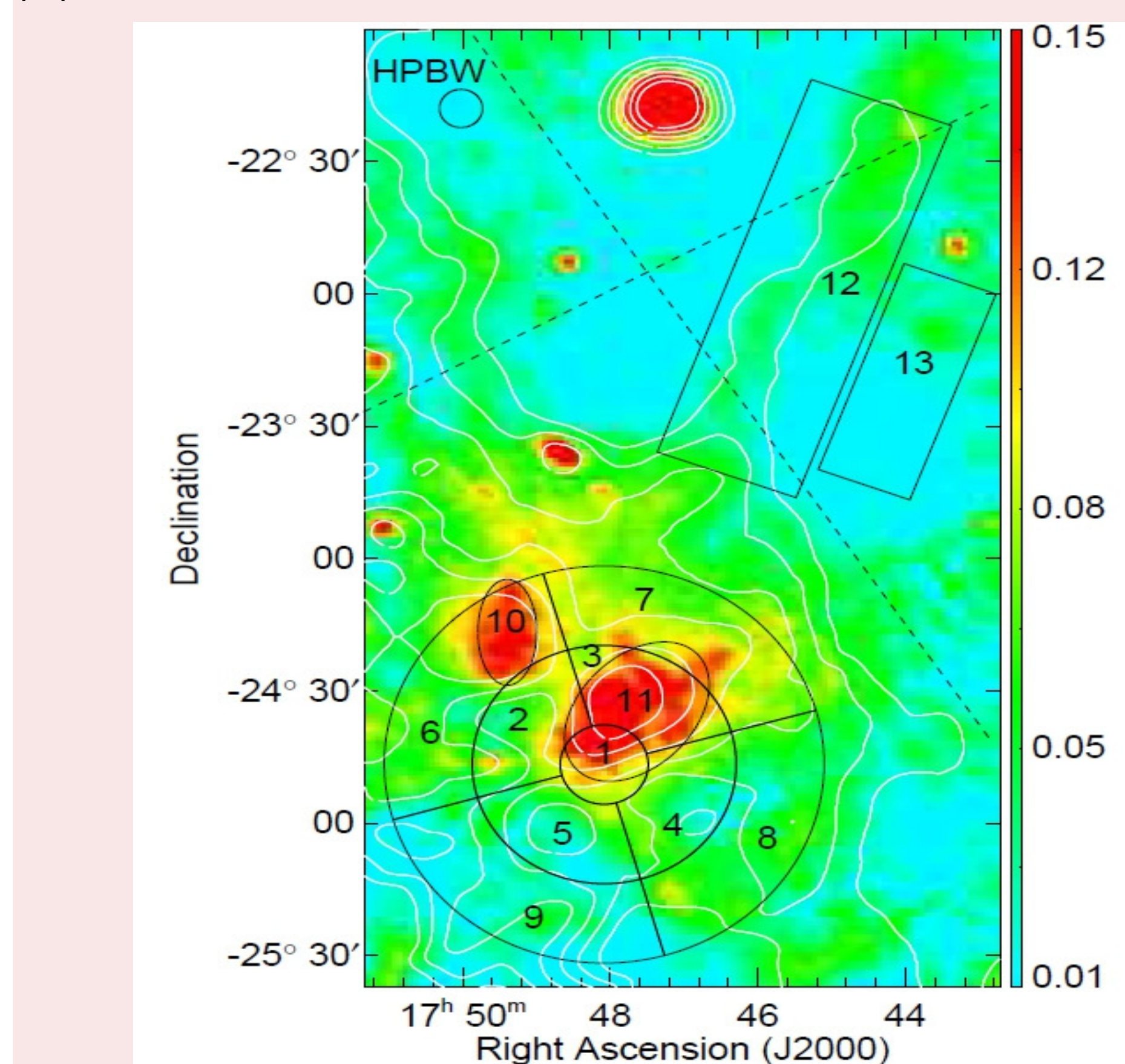

Figure 1: *Radio map from the Effelsberg Galactic Plane. From Clapson et al. (2011)*

2.2. New Radio Map at $\lambda = 6$ cm

We performed 4.85 GHz observations over three consecutive nights between 2011 April 30 and 2011 May 2 using the 100-m Effelsberg Radio Telescope. The most interesting feature seen in our new 6-cm map is a large-scale structure ($\sim 20'$ in length) north of Terzan 5. We estimated its flux density, using the box-shaped region indicated in Figure 2, as 277.5 ± 19.6 mJy. The origin of this emission is unknown, but this may be due to the interaction of particles escaping from the cluster with the B-field of the interstellar medium. While this new detection is intriguing, we do not attempt to fit the relatively low flux of this large new structure. Rather, we follow Clapson et al. (2011) and assume that the radio emission from their smaller-scale "Region 11" may be due to electrons injected by the population of embedded MSPs. We fit this using a diffuse low-energy synchrotron radiation (LESR) component due to the interaction of these relativistic electrons with the cluster B-field.
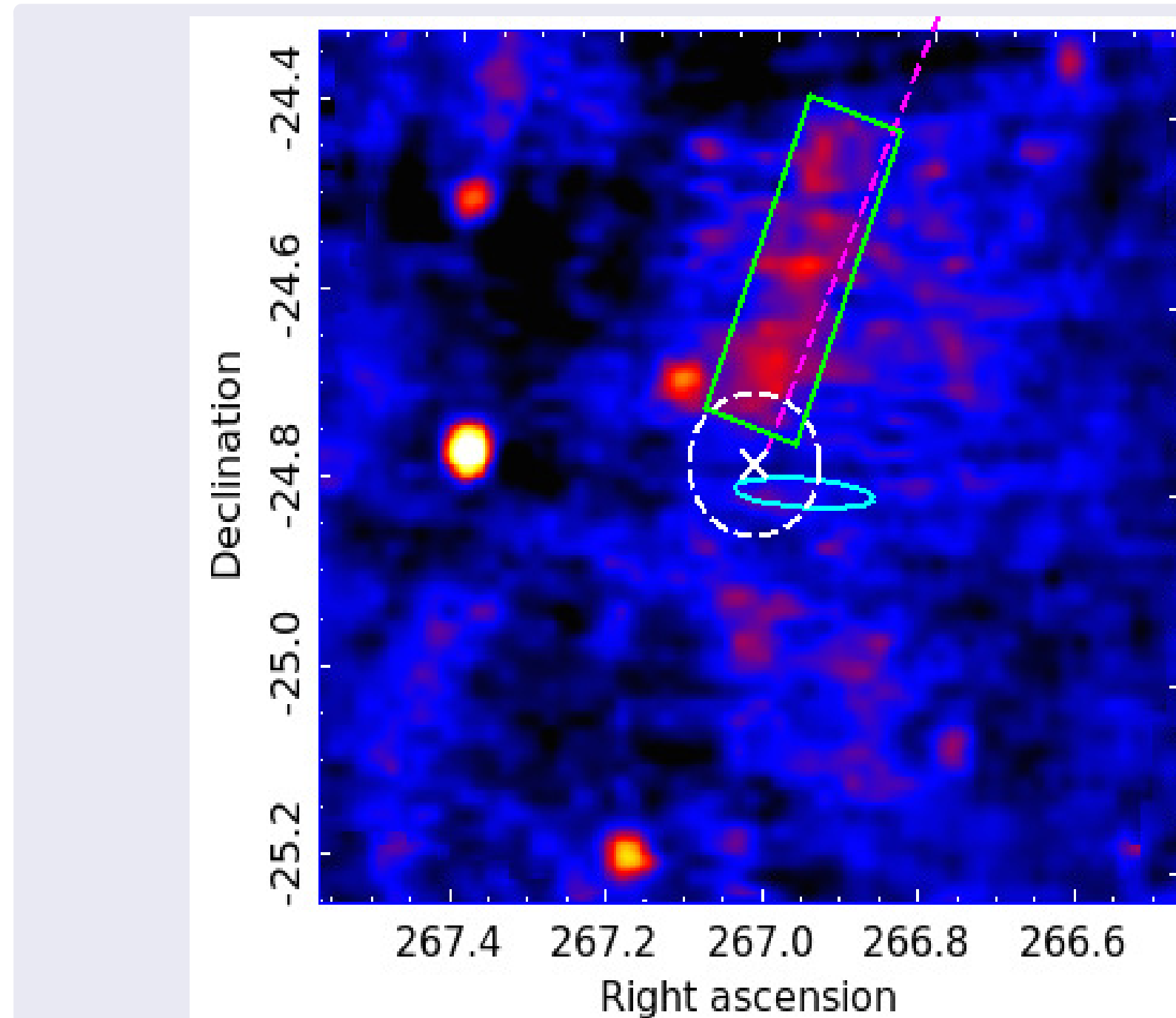

Figure 2: *The 4.85 GHz flux map from the observation with the Effelsberg Radio Telescope. The position of Terzan 5 is marked with a cross (white). The dashed circle (white) shows the tidal radius of the GC. The ellipse (cyan) shows the intrinsic size of the TeV source detected with H.E.S.S. The dashed line (magenta) indicates the direction of the large-scale elongated radio feature found in the Effelsberg 11 cm survey map (see Clapson et al. 2011, their "Region 12"). The box (green) shows the region used for the flux measurement from the newly discovered extended feature.*

2.3. Optical Upper Limits: Comparison of Thermal and non-Thermal Flux Levels

The predicted LESR component's flux is relatively low in the optical band (Kopp et al. 2013), and we show that it may be difficult to directly observe this component since there are $\sim 10^5$ stars that contribute a high level of blackbody (BB) radiation that will swamp any diffuse non-thermal emission. We use the surface-density profile of Terzan 5 obtained by Trager et al. (1995), as converted by Cohn et al. (2002) to obtain the BB flux from stars in different annuli (as defined by Cohn et al. 2002) centered on the cluster, and also the total flux expected from the full cluster. We estimate the thermal νF_ν flux level:

$$\frac{B_\nu < \nu > A_\star}{d^2} = \frac{8\pi R^2 h < \nu >^4}{d^2 c^2} \frac{N_{\text{ann}}}{e^{\frac{h\nu}{k_B T}} - 1}$$
$$\sim 1.7 \times 10^{-11} R_{10}^2 \, \text{erg cm}^{-2} \text{s}^{-1},$$

with $R_{10} = R/10^{10}$ cm and assuming $d = 5.9$ kpc. For the whole cluster with $N_\star = N_{\text{ann}} = 7.7 \times 10^4$, we find that the predicted BB flux is $\sim 6.2 \times 10^{-8} \text{erg cm}^{-2} \text{s}^{-1}$, while the predicted νF_ν flux for the LESR at 1 eV is only $\sim 7.2 \times 10^{-13} \text{erg cm}^{-2} \text{s}^{-1}$. We find that the flux ratio (BB/SR) of 10^5 for all annuli drops from $\sim 10^5$ to $\sim 10^3$ with increasing radius, out to $\sim 0.35 R_t$, with R_t the tidal radius.

2.4. Diffuse X-ray Emission

Eger et al. (2010) searched for extended diffuse X-ray emission from Terzan 5. They extracted spectra from 8 concentric annular regions centered on the cluster core to measure the level of diffuse X-ray emission around it, and discovered significant excess emission above the particle background level. The diffuse X-ray signal is extended well beyond the half-mass radius of the cluster and the surface brightness appears to be peaked at the GC center and decrease smoothly outwards (see region 1 to region 6 in Figure 3).
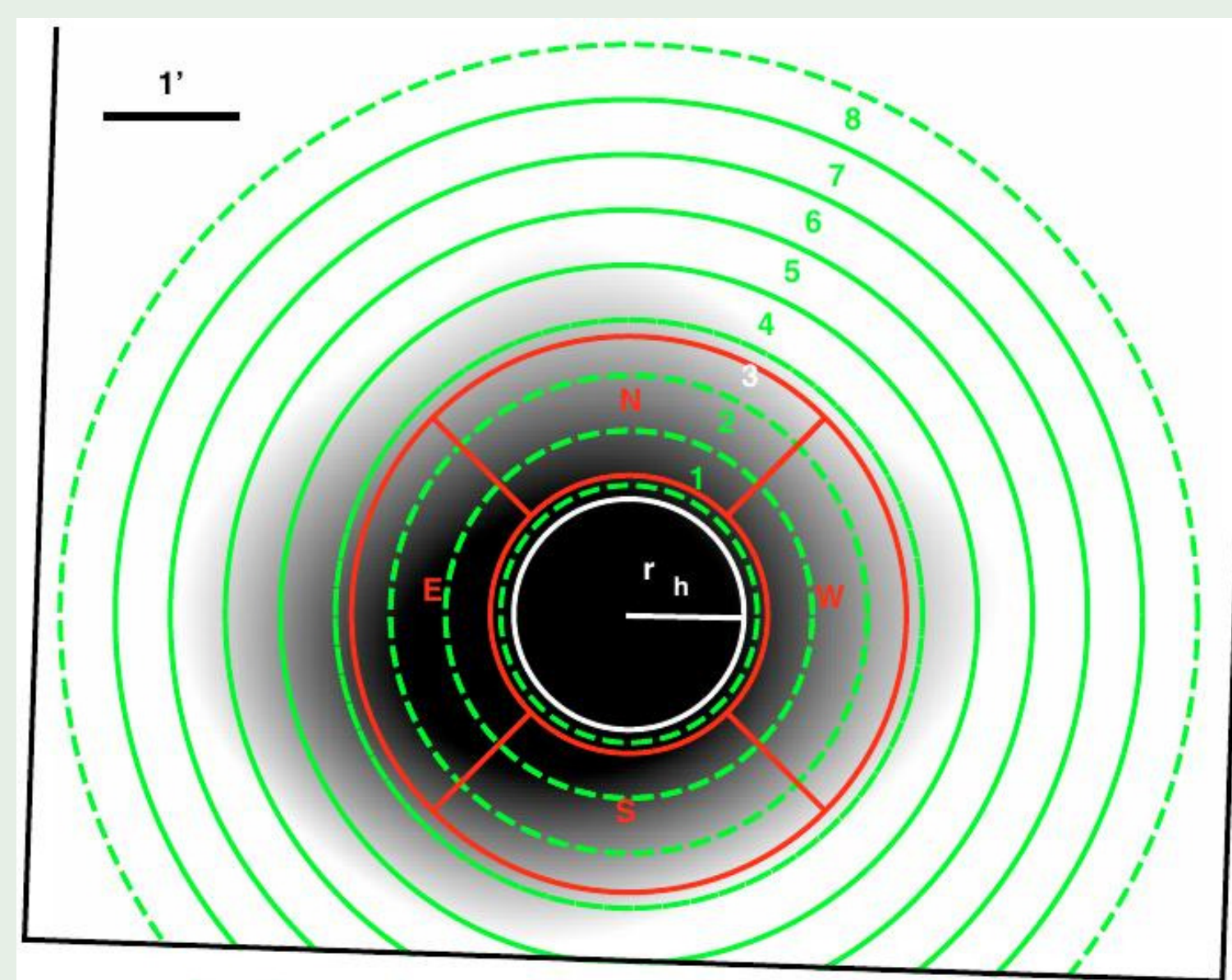

Figure 3: *Smoothed, exposure corrected and non-X-ray background (NXB) subtracted Chandra image of diffuse X-ray emission in the $1-7$ keV band around Terzan 5. Shown are the eight annular extraction regions (dashed green lines, numbered 1 to 8) and the four pie-shaped regions (solid red lines, labeled N, E, S and W).*

2.5. New *Fermi* LAT Data Analysis

Terzan 5 was the second GC to be associated with a *Fermi* LAT source. Abdo et al. (2010) estimated the number of MSPs in this cluster to be approximately 180 using an estimate of the average MSP spin-down power and gamma-ray efficiency with measured gamma-ray flux. We obtained new *Fermi* data that proved constraining for the low-energy tail of the unpulsed IC component (see Figure 4).

2.6. H.E.S.S. Data

H.E.S.S. discovered a VHE γ-ray source in the direction of Terzan 5 (Abramowski et al. 2011). No new observations have been carried out on this source since its discovery.

3. MODELING THE BROADBAND SED

3.1. Leptonic Modeling of the Broadband SED of Terzan 5: LESR and IC Components

We used a multi-zone, steady-state, spherically symmetric model that assumes pulsars to be the sources of relativistic leptons in the GCs to calculate the particle transport and to predict the SED from GCs for a very broad energy range by considering unpulsed synchrotron radiation (SR), as well as inverse Compton (IC) emission (blue dashed lines).
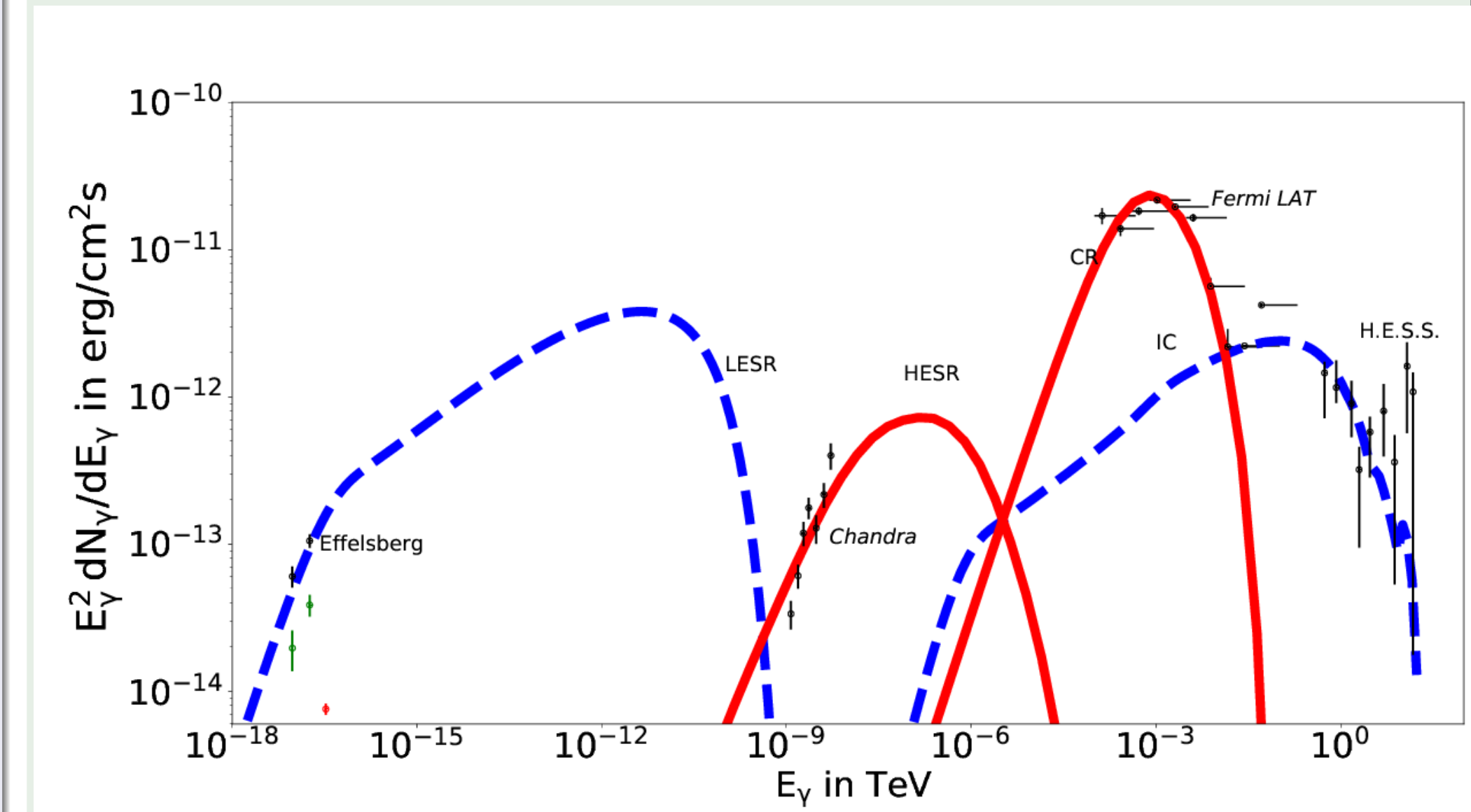

Figure 4: *Different spectral components for Terzan 5 predicted by the leptonic models of Kopp et al. (2013), and Harding et al. (2008); Harding & Kalapotharakos (2015). We assumed minimum particle energy $E_{\text{min}} = 0.01$ TeV, maximum particle energy $E_{\text{max}} = 20$ TeV, injected spectral normalisation $Q_0 = 1.35 \times 10^{34} \text{erg}^{-1} \text{s}^{-1}$, magnetic field $B = 4.0 \,\mu$G, injected spectral index $\Gamma = 1.5$, number of MSPs $N^C_{\text{MSPs}} = 74$, and diffusion coefficient $\kappa = 7 \times 10^{-5}$ kpc^2/Myr. The HESR and CR components are predictions using the model of Harding et al. (2008); Harding & Kalapotharakos (2015) for $\alpha = 45°$, $\zeta = 60°$, $< P > = 7.7 \times 10^{-3}$ s, and $B_{\text{surf}} = 5.8 \times 10^9$ G. We also indicate Chandra (Eger et al. 2010), H.E.S.S. (Abramowski et al. 2011), and radio data (Clapson et al. 2011; and this work). The black points are for Region 11, green points for Region 1 and red point for Region 12.*

3.2. Pair high-energy SR (HESR) and Primary CR Components

Following the idea of Kopp (2013), we propose the X-ray data point to a new component that has not been considered before. We use a model of Harding & Kalapotharakos (2015) and assumed that electron-positron pairs radiate pulsed SR (lower-energy red solid line). Given the much higher local B-field (e.g., the magnetospheric field at the MSP light cylinder $B_{\text{HESR}} \sim 10^6$ G vs. the GC field $B_{\text{LESR}} \sim 10^{-5}$ G) and the much smaller average pitch angle α (~ 0.1 vs. $\sim \pi/2$ radians) as well as different particle energies, the cutoff energy of this new component is much higher than that of the LESR spectrum:

$$\frac{E_{\text{HESR}}}{E_{\text{LESR}}} \sim \left(\frac{\gamma_{\text{SR}}}{\gamma_{\text{LESR}}}\right)^2 \frac{B_{\text{HESR}} \sin \alpha_{\text{HESR}}}{B_{\text{LESR}} \sin \alpha_{\text{LESR}}}$$
$$\sim 10^4.$$

Using the same model we fit the *Fermi* LAT data by calculating the cumulative primary CR component of pulsed γ-ray emission.

3.3. MSP Population Energetics

We modeled the underlying (visible and invisible) pulsar population via a parametric spin-down luminosity function $dN/d\dot{E} = N_0 (\dot{E}/\dot{E}_0)^{-1+\gamma_L}$ (Johnston & Verbunt 1996). By using the observed and estimated unobserved non-thermal X-ray luminosity (Eger et al. 2010) plus the Chandra point-source detection sensitivity, and by fixing the average MSP spin-down luminosity to $< \dot{E} > = 9 \times 10^{34} \text{erg s}^{-1}$, we could balance the X-ray emission using a radiation efficiency of $\eta_X = 0.063\%$, $\dot{E}_{\text{min}} = 3 \times 10^{31} \text{erg s}^{-1}$, $\dot{E}_{\text{max}} = 3 \times 10^{35} \text{erg s}^{-1}$, $\gamma_L = -0.04$, total pulsars $N^X_{\text{tot}} = 38$. This solution yields $N^X_{\text{vis}} = 15$ visible pulsars, $N^X_{\text{invis}} = 23$ invisible pulsars, and $\langle \dot{E} \rangle_{\text{invis}} \sim 2 \times 10^{33} \text{erg s}^{-1}$. A different choice of η_X (or $\langle \dot{E} \rangle_{\text{vis}}$) will lead to a different solution. Future constraints on N^X_{vis} and $\langle \dot{E} \rangle_{\text{vis}}$ may help constrain the pair mulitplicity $M_\pm$.

4. CONCLUSION

We found a reasonable fit to the broad band spectrum of Terzan 5. Future constraints on low-energy tail of the LESR component may ultimately provide insight into the (re)acceleration mechanisms of particles in the GC. The CTA may provide some aid in constraining the low-energy tail of the IC component by lowering the energy threshold as well as having a lower sensitivity.

REFERENCES
Abdo, A. A., Ackermann, M., Ajello, M. et al. 2010, A&A, 524, A75
Abramowski, A., Acero, F., Aharonian, F. et al. 2011, ApJ, 735, 12
Abramowski, A., Acero, F., Aharonian, F. et al. 2013, A&A, 551, A26
Aharonian, F. Akhperjanian, A. G., Anton, G., et al. 2009, A&A, 499, 273
Anderhub, H., Antonelli, L. A., Antoranz, P. et al. 2009, ApJ, 702, 266
Cadelano, M., Ransom, S. M., Freire, P. C. C., Ferraro, F. R., Hessels, J. W. T., Lanzoni, B., Pallanca, C., & Stairs I. H. 2018, ApJ, 855, 125
Clapson, A.-C., Domainko, W., Jamrozy, M. et al. 2011, A&A, 532, 47
Cohn, H. N., Lugger, P. M., Grindlay, J. E., & Edmonds, P. D. 2002, ApJ, 571, 818
Condon, J. J., Cotton, W. D., Greisen, E. W. et al. 1998, AJ, 115, 1693
Eger, P., Domainko, W., & Clapson, A.-C. 2010, A&A, 513, A66
Harding, A. K., Stern, J. V., Dyks, J., & Frackowiak, M. 2008, ApJ, 680, 1378
Harding, A. K., & Kalapotharakos, C. 2015, ApJ, 811, 63
Johnston, H. M & Verbunt, F. 1996, A&A, 312, 80
Kopp, A., Venter, C., Büsching, I., & de Jager, O. C. 2013, ApJ, 779, 126
McCutcheon M et al. 2009 Proc. 31st ICRC, Lodz, Poland (arXiv:0907.4974)
Ndiyavala, H., Krüger, P. P., & Venter, C. 2018, MNRAS, 473, 397
Trager, S. C., King, I. R., & Djorgovski, S. 1995, AJ, 109, 218
Valenti, E., Ferraro, F. R., & Origlia, L. 2007, ApJ, 133, 1287
Verbunt, F., & Hut, P. 1987, in IAU Symp. 125, The Origin and Evolution of Neutron Stars, ed. D. J. Helfand & H. H. Huang (Dordrecht: Reidel), 187